Received: 25 March 2021 | Revised: 4 August 2021 | Accepted: 4 August 2021

DOI: 10.1002/mbo3.1232

ORIGINAL ARTICLE

MicrobiologyOpen Open Access WILEY

Efficiency of the synthetic self-splicing RiboJ ribozyme is robust to *cis*- and *trans*-changes in genetic background

Markéta Vlková | Bhargava Reddy Morampalli | Olin K. Silander

School of Natural and Computational Sciences, Massey University, Auckland, New Zealand

Correspondence
Markéta Vlková and Olin K. Silander, School of Natural and Computational Sciences, Massey University, Auckland, New Zealand.
Emails: marketa.m.vlkova@gmail.com (M.V.); olinsilander@gmail.com (O.K.S.)

Funding information
Royal Society Te Apārangi, Marsden Fund, Grant/Award Number: MAU1703

Abstract

The expanding knowledge of the variety of synthetic genetic elements has enabled the construction of new and more efficient genetic circuits and yielded novel insights into molecular mechanisms. However, context dependence, in which interactions between *cis*- or *trans*-genetic elements affect the behavior of these elements, can reduce their general applicability or predictability. Genetic insulators, which mitigate unintended context-dependent *cis*-interactions, have been used to address this issue. One of the most commonly used genetic insulators is a self-splicing ribozyme called RiboJ, which can be used to decouple upstream 5′ UTR in mRNA from downstream sequences (e.g., open reading frames). Despite its general use as an insulator, there has been no systematic study quantifying the efficiency of RiboJ splicing or whether this autocatalytic activity is robust to *trans*- and *cis*-genetic context. Here, we determine the robustness of RiboJ splicing in the genetic context of six widely divergent *E. coli* strains. We also check for possible *cis*-effects by assessing two SNP versions close to the catalytic site of RiboJ. We show that mRNA molecules containing RiboJ are rapidly spliced even during rapid exponential growth and high levels of gene expression, with a mean efficiency of 98%. We also show that neither the *cis*- nor *trans*-genetic context has a significant impact on RiboJ activity, suggesting this element is robust to both *cis*- and *trans*-genetic changes.

KEYWORDS
insulation, RiboJ, ribozyme, RT-qPCR, splicing

1 | INTRODUCTION

Synthetic nucleic acid functional elements used to control protein output—such as promoters, ribosome binding sites, or terminators—are an indispensable part of engineered genetic circuits (Levskaya et al., 2005; Na et al., 2013; Neves et al., 2020) and are frequently used to study basic biological processes (Barbier et al., 2020; Bittihn et al., 2020). The value of such synthetic functional elements increases as their properties are better described and quantified—in some cases, careful quantification of the behavior of synthetic functional elements has led to fundamentally new insights into molecular mechanisms controlling protein output (Schmiedel et al., 2019; Urtecho et al., 2019).

One important type of synthetic functional elements that have been used to ensure predictable and robust protein output from mRNA are self-splicing ribozymes. These ribozymes can be used to splice mRNA at specific locations, for example, to remove the 5′ untranslated region (UTR). One of the most common ribozymes used to remove 5′ UTRs is RiboJ. By removing the 5′ UTR of the mRNA, RiboJ enables transcripts having different promoters and

thus different 5′ UTRs to produce identical mRNAs. This mitigates any effects that the 5′ UTR might have on mRNA folding or ribosome binding, keeping the translation initiation rate consistent (and predictable) even when promoters have different sequences (Neves et al., 2020; Urtecho et al., 2019; Yu et al., 2018). The utility of the RiboJ element was first demonstrated when it was used to ensure predictable expression in a synthetic NOT gate circuit, irrespective of the sequence of the promoter used to control the expression of a CI repressor in the system (Lou et al., 2012).

However, since the first use of RiboJ as a means of ensuring predictable expression, additional research has suggested there can also be unexpected effects of its use. Clifton et al. (2018) demonstrated that RiboJ insertion into the mRNA sequence led to an increase in protein expression and that the relative increase in expression depended on the strength of the promoter used. This effect was attributed to hairpin formation at the 5′ end of mRNA whose 5′ UTR had been removed by RiboJ, leading to higher stability and increased translation (Carrier & Keasling, 1997; Clifton et al., 2018; Neves et al., 2020). Another unexpected effect was observed when Bartoli et al. (2020) designed a tunable system to control translation initiation via binding of small regulatory RNA (sRNA). The complex secondary structure of mRNA molecules with RiboJ at the 5′ end appeared to interfere with the sRNA binding, decreasing the performance of the system. These results emphasize that unknown properties and behaviors of synthetic functional elements—here, RiboJ in particular—can lead to unexpected obstacles when creating new synthetic circuits.

We hypothesized that a complicating factor in the use of the RiboJ system would be the varying efficiency of RiboJ autocatalytic splicing activity between different bacterial strains, or due to polymorphisms near the RiboJ element. To our knowledge, there has been no systematic study quantifying the efficiency of the autocatalytic RiboJ splicing, or whether the efficiency of this autocatalytic activity depends on the genetic background of the organism in which it is used. To address these questions we first developed an assay to quantify RiboJ self-splicing efficiency. We then tested the robustness of the self-splicing activity to *cis*-genetic changes by assaying efficiency in two genetic contexts that differ by a single nucleotide polymorphism (SNP) close to the autocatalytic site of RiboJ. Finally, we tested the robustness of RiboJ behavior to *trans*-genetic changes by quantifying efficiency in six widely divergent strains of *E. coli*.

2 | EXPERIMENTAL PROCEDURES

2.1 | Bacterial strains

The genetic backgrounds of *E. coli* strains used in this study are listed in Table 1. The identity of all lab strains was confirmed using whole-genome sequencing. The whole genomes of strains SC312 and SC392 have been also sequenced (Breckell & Silander, 2020). Four different plasmids (Table 2) were transformed into each of the strains, providing 24 clones that we used to evaluate the efficiency of RiboJ splicing. The presence of the plasmids with correct inserts in all clones was confirmed by Sanger sequencing (Macrogen, South Korea).

2.2 | Plasmid construction

All plasmids used to measure the autocatalytic activity of RiboJ are listed in Table 2. Plasmids p69A.RJ− and p69C.RJ− were generously gifted by D. Blank, University of Basel. Plasmids p69A.RJ+ and p69C.RJ+ were constructed using plasmid pMV001 (which was created beforehand), as follows: RiboJ was ordered as four 60nt single-stranded oligos with each 30nt of them being homologous to either another 60nt RiboJ oligo or PCR amplified pUA66 vector (Table A1). These four oligos were then assembled with PCR amplified pUA66 vector using NEBuilder HiFi DNA assembly kit (New England Biolabs). The resulting pMV001 plasmid assembly mix was then used to electroporate Top10 *E. coli* cells (Invitrogen). The presence of the RiboJ was then confirmed by Sanger sequencing (Macrogen, South Korea) from colonies grown on selective LB agar plates with 50 μg/ml Kanamycin.

To create inserts for p69A.RJ+ and p69C.RJ+ plasmids the *lacZ* promoter regions from p69A.RJ− and p69C.RJ− were PCR amplified.

TABLE 1 Bacterial strains used in this study

Bacterial strains			
Strain	**Relevant characteristics**	**Phylogroup**	**Source or reference**
SC392	*A natural isolate of E. coli; Soil; 7/18/05; SC15-U2out14; St. Louis Clyde; Upshore (2m) outside the box*	B1	(Ishii et al., 2006)
SC312	*A natural isolate of E. coli; Water; 6/15/05; SC14-W8; St. Louis Clyde; Surface water*	B1	(Ishii et al., 2006)
MG1655	*F− λ− ilvG− rfb−50 rph−1*	A	(Blattner et al., 1997)
DH5α	*F− φ80lacZΔ M15 Δ (lacZYA-argF) U169 recA1 endA1 hsdR17 (rK− mK+) phoA supE44 λ− thi−1 gyrA96 relA1*	A	Invitrogen
BW25113	*F− DE(araD−araB)567 lacZ4787(del)::rrnB−3 LAM− rph−1 DE(rhaD-rhaB)568 hsdR514*	A	(Datsenko & Wanner, 2000)
BL21 Star (DE3)	*F-ompT hsdSB (rB−, mB−) galdcmrne131 (DE3)*	A	Invitrogen

TABLE 2 Plasmids used in this study

Plasmids		
Plasmid	**Relevant characteristics**	**Source**
p69A.RJ−	*lacZ* promoter 69A, without RiboJ	D. Blank, University of Basel
p69C.RJ−	*lacZ* promoter 69C, without RiboJ	D. Blank, University of Basel
p69A.RJ+	*lacZ* promoter 69A, with RiboJ	This study
p69C.RJ+	*lacZ* promoter 69C, with RiboJ	This study

Note: All plasmids carry Kan^R selection marker and were created using pUA66 backbone (Zaslaver et al., 2006).

The primers used contain 17nt overhangs that are homologous to PCR amplified pMV001 vector (Table A1). We ligated the vector with the inserts through Gibson assembly (Gibson et al., 2009) using the NEBuilder HiFi DNA assembly kit (New England Biolabs). All primers and oligos used including sequencing primers (Integrated DNA Technologies) are listed in Table A1. In all cases, the same method for insert and vector PCR amplification from existing plasmids was used as described by (Li et al., 2011).

2.3 | Flow cytometry

Strains for flow cytometry were grown in M9 minimal media (Sigma) supplemented with $MgSO_4$, $CaCl_2$, 0.4% (w/v) carbon source (glucose, galactose, or lactose), and 50 μg/ml Kanamycin. They were first inoculated from a glycerol stock library into a 96 well microplate using a pin replicator (Enzyscreen B.V.) and incubated at 37°C. After overnight incubation, the cultures were diluted into the same fresh media with the pin replicator and incubated the same way until they reached the mid-exponential phase (~4 h). At that point, the cells were diluted into 1× PBS with ~1% formaldehyde and kept on ice until measuring the GFP levels using the flow cytometer.

Cytometry was performed with a BD FACSCanto II and BD FACSDiva software version 6.1.3. The GFP fluorescence was measured using the 488 nm laser and a 513/17 nm bandpass filter. The data from FACSDiva were exported into Flow Cytometry Standard files, and cell gating and fluorescence analysis was performed using custom R scripts (flowCore package version 2.0.1; the scripts are available through https://doi.org/10.5281/zenodo.5154246). Cells were gated based on their maximal kernel density of forward and side scatter values, keeping about ⅓ of all events. The modal fluorescence was calculated from gated cells as the maximal kernel density from the fluorescence signal.

2.4 | RNA isolation

RNA was isolated from four clones a day, while clones with the same genetic background were processed together on the same day. We isolated RNA from MG1655 clones twice on two different days, all other clones were isolated just once. Each strain containing one of the four plasmids (Table 1 and Table 2) was grown from a single colony overnight in 3 ml of LB with 50 μg/ml Kanamycin and 2 mM IPTG (Isopropyl β-D-1-thiogalactopyranoside) with shaking (250 rpm) at 37°C. Because the high IPTG concentration impaired the growth of SC312 strain with RiboJ plasmids (i.e., p69A.RJ+ and p69C.RJ+), we grew all SC312 clones for RNA isolation in LB with 0.2 mM of IPTG instead. The next day 15 ml of the same fresh media in 50 ml Falcon tubes was inoculated by 15 μl of this overnight culture. This was incubated under the same conditions. Once the cultures reached an exponential phase (between 1.75 h and 2.5 h) it was placed on an ice slurry.

Next, we added 7.5 ml of ice-cold 5% phenol in ethanol to each 15 ml of culture and kept them on ice for 15 min. The cultures were then spun at 7000G for 7 min at 4°C, the supernatant was discarded and the pellet was redispersed in 350 μl of 3 mg/ml Lysozyme solution (in TE buffer). After incubating for 3 min, an equal volume of RNA lysis buffer was added and RNA isolated using Monarch Total RNA Miniprep Kit (New England Biolabs). Each sample was treated by DNase I twice: (1) on-column during the RNA extraction and then (2) in-tube after RNA extraction. This was done to avoid any amplification from residual gDNA during RT-qPCR. After the second treatment with DNase I the samples were column-purified and concentrated using RNA Clean & Concentrator-5 kit (Zymo Research). The quality of RNA in each sample was checked on 1% agarose gel and its concentration was measured on a Qubit 4 fluorometer (Invitrogen). The isolated RNA samples were then stored in a −80°C freezer.

2.5 | RT-qPCR

To assess the efficiency of PCR amplification by our primers we used RNA from MG1655 strain (all four plasmids). A ten-fold serial dilution was performed on all the RNA samples up to 10^{-4}. RT-qPCR was run on all the dilutions in triplicates using two different master mixes differing by the forward primer used—F1 and F2 (Figure 2 and Table A1). The total reaction volume was 20 μl with 2 μl of template RNA. We used SensiFAST Probe No-ROX One-Step Kit (Meridian Bioscience) and PikoReal Real-Time PCR System (Thermo Scientific) with following cycling conditions: Reverse transcription for 10 min at 45°C; Polymerase activation for 2 min at 95°C; 40 cycles of denaturation for 5 s at 95°C and Annealing & extension for 20 s at 55°C. The C_t values were obtained via PikoReal software version

2.2, exported into .xlsx file, and converted into .csv to be further analyzed using custom R scripts (available through https://doi.org/10.5281/zenodo.5154246).

To assess the autocatalytic efficiency of RiboJ, the RNA from all samples was first diluted from its original concentration (~2–3 μg/μl) to 20 pg/μl to obtain C_t values between 20 and 40 and to dilute out any potential residual of gDNA (to less than one molecule per reaction). We confirmed that no amplification occurred when omitting reverse transcriptase from the master mix. Each RNA sample was then run in three or more replicates using both primer sets (Figure 2) with the same conditions described above. We exported the data from the PikoReal software version 2.2 into .xlsx files, converted these into .csv, and performed all analyses using custom R scripts (available through https://doi.org/10.5281/zenodo.5154246). In brief, we determined the mean C_t value of all the replicates for the uncut and cut RiboJ transcripts and calculated the efficiency as the ratio of the cut and uncut transcripts using the Pfaffl method (Pfaffl, 2001):

$$\text{Eff} = 100 - 100 * \frac{E^{(a-b)}}{E^{(c-d)}}$$

where E is constant mean amplification efficiency (1.95766), a and b are mean C_t values of transcripts without and with RiboJ, respectively, using F1 primer, and c and d are mean C_t values of the same transcripts using F2 primer. To obtain a measure of the error in these estimates, we bootstrapped the data 10,000 times and recalculated the ratio for each bootstrap replicate.

2.6 | Plasmid sequencing

Plasmid DNA was isolated from overnight cultures using the StrataPrep Plasmid Miniprep Kit (Agilent), per the manufacturer's instructions. These were then prepared for Oxford Nanopore sequencing using the Oxford Nanopore rapid barcoding library prep, per the manufacturer's instructions, with a separate barcode used for each plasmid. These were run on a single MinION flowcell for 1 h and 50 min. The reads were base-called using the guppy_basecaller v5.0.7 high accuracy model and demultiplexed using guppy_barcoder, resulting in between 28.8 Mbp and 35.1 Mbp for each plasmid. These reads were used as input for medaka, using medaka_consensus to correct the original plasmid sequence.

3 | RESULTS

Our first motivation for quantifying the behavior of RiboJ arose during experiments aimed at understanding the effects of promoter polymorphisms segregating in the environmental *E. coli* population on transcription and translation. Here, "promoter" is defined as the entire intergenic region upstream of an open reading frame, as well as part of the upstream and downstream open reading frames

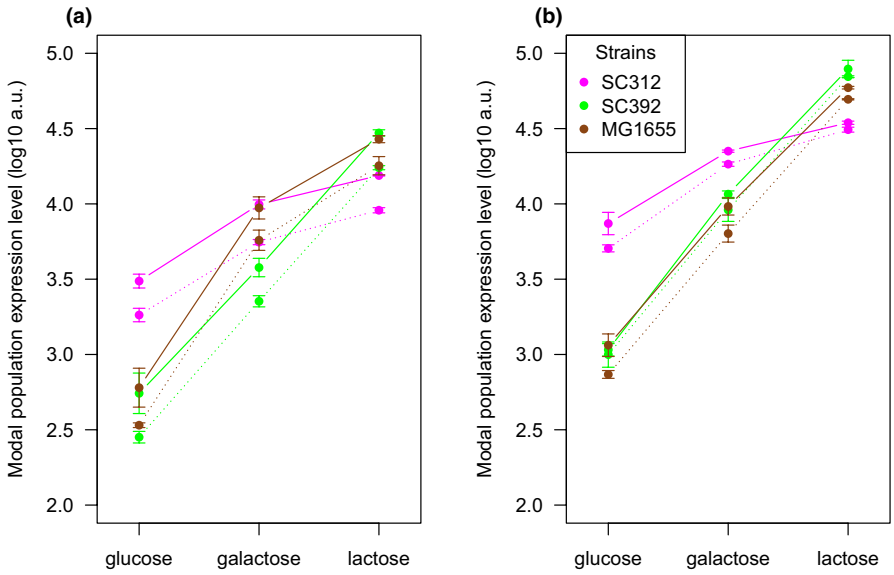

FIGURE 1 Modal expression levels differ consistently due to a single A to C change at position +69 of the *lacZ* open reading frame both without RiboJ (a) and with RiboJ (b) and across genetic backgrounds. Shown are the modal population fluorescence levels for GFP driven by an upstream *lacZ* promoter for three divergent strains of *E. coli*. In all genetic backgrounds tested and all growth conditions (glucose, galactose, and lactose), the fluorescence levels from a promoter with the 69C polymorphism (dotted line) were consistently lower than those from the promoter with the 69A polymorphism (solid line). On the log10 scale that is shown, a 0.1 difference is equivalent to a 25% change in expression. There are clear effects of genetic background on both the level and dynamic range of protein expression. In particular, SC312 has a narrow dynamic range, with relatively high expression in non-lactose environments compared to the other strains, but relatively low expression in lactose. Despite this, the effect of the A to C change is nearly constant. Whiskers show one standard deviation of three replicates

(Zaslaver et al., 2006). We include parts of the upstream and downstream open reading frames as it is well established that many open reading frames contain transcriptional regulatory elements affecting their own regulation or that of downstream genes. We assay the effects of the promoter on transcription by quantifying the fluorescence that occurs due to a GFP open reading frame that lies downstream of this "promoter".

In the case of the *lacZ*, here we define the "promoter" as the *lacI-lacZ* intergenic region, plus 88 and 71 bp of each flanking upstream (*lacI*) and downstream (*lacZ*) coding regions, respectively. We discovered a single SNP at position 69 relative to the *lacZ* gene start codon (C to A) that resulted in a change in downstream protein levels. We found that the effect of this SNP on GFP protein expression was consistent in different genetic backgrounds as well as during growth in different carbon sources (Figure 1a and Figure A1a). To check whether this C69A SNP affected transcription or translation (or both), we incorporated RiboJ as an insulator downstream of it (Figure 2, Top panels). This ensured that the mRNA being translated was identical regardless of which SNP was present. Thus, if the change in protein expression remained in the presence of RiboJ, we could infer that the change was due solely to the SNP affecting transcription. If the difference disappeared in the presence of RiboJ, we could infer that the change was due to the SNP affecting translation. However, it was also possible that the SNP itself interfered with RiboJ cutting (a *cis*-effect). If so, we could not unambiguously infer that the cause of the changes in fluorescence we observed was due to translation or transcription (or both). In addition, the genetic background of the strain itself might have affected RiboJ cutting (a *trans*-effect). To exclude the possibility of *cis*- or *trans*-effects on RiboJ cutting efficiency, we quantified efficiency in the presence of *cis*- and *trans*-genetic changes.

We designed an RT-qPCR assay to quantify the autocatalytic cutting activity of RiboJ. This assay is based on the principle that for a pair of forward and reverse primers that span the RiboJ cut site, an amplification product should only be produced for uncut mRNA molecules. In contrast, for primer pairs that do not span the cut site, an amplification product should be produced for all molecules. By examining the relative numbers of cut and uncut molecules, we can infer the efficiency of RiboJ cutting relative to the rate of production of all transcripts controlled by the same promoter (i.e., the rate of transcription). To this end, we designed two qPCR primer sets. The first set produced an amplicon from a region spanning the RiboJ cut site, while the second produced an amplicon from a region downstream of the RiboJ cut site (Figure 2). Both sets shared the same reverse primer, differing solely by the location of the forward primer. Because one forward primer binds upstream of the RiboJ cut site, no amplification can occur if the 5′ UTR sequence has been cut off (Figure 2, Middle panel). The second forward primer binds downstream of the cut site

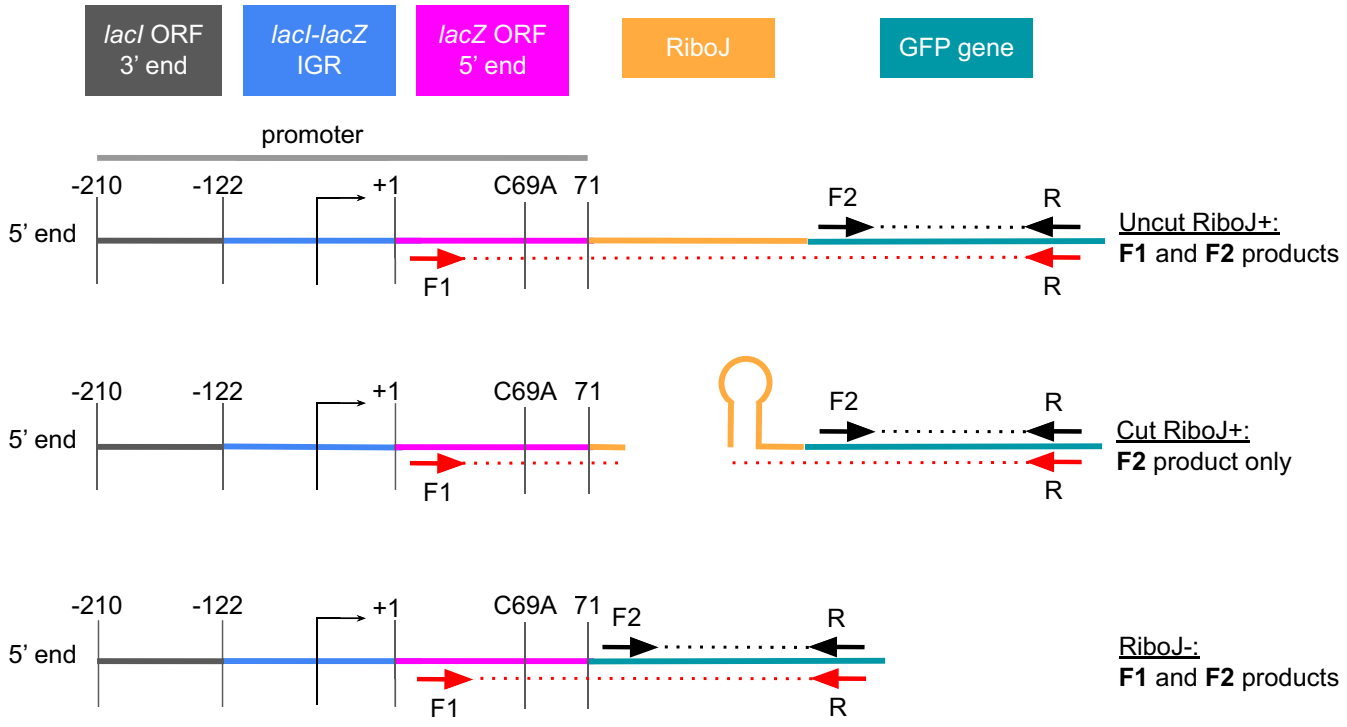

FIGURE 2 Scheme of the RT-qPCR primer design to quantify the efficiency of RiboJ cutting. Each primer is represented by an arrow, with pairs colored the same. The dotted lines indicate amplicons. If the dotted line between a primer pair is interrupted, the amplicon is not produced. When RiboJ cleaves off the 5′ UTR (Middle panel), the amplicon from primer F1 is not produced, while the amplicon from the F2 primer is still produced. The *lacI-lacZ* intergenic region (IGR) with the first 71 bp and last 88 bp of the *lacZ* and *lacI* open reading frames, respectively, were placed upstream of GFP (and RiboJ) as a promoter. The arrow in the middle of *lacI-lacZ* IGR indicates the transcription start site. The translation is driven from a strong synthetic ribosome binding site downstream of the *lacZ* gene sequence (here as a part of the GFP gene)

and results in an amplification product from all transcripts. To quantify differences in amplification that might result from primer binding or other unforeseen mechanisms, we calculated the relative fold change in the abundance of these two amplicons when RiboJ is absent. In the absence of RiboJ, any difference in amplification between the two primer sets should be due solely to differences in primer efficiency or related effects, as without RiboJ, both amplification products will always be produced (Figure 2, bottom panel).

We first assessed whether *trans*-genetic changes affected the self-splicing activity of RiboJ, by assaying RiboJ activity in six widely divergent strains of *E. coli* (Table 1). To test for *cis*-effects, we assayed activity in two promoter contexts, each varying by a single SNP that was 8 bp upstream of the RiboJ cut site (2 bp upstream of RiboJ sequence). We thus transformed each of the six strains with each of four plasmids differing by the C69A SNP in the *lacZ* promoter and either with RiboJ or without RiboJ (Figure 2, Table 2). We isolated RNA from exponentially growing cultures for all strains and confirmed that the amplification efficiency of all primer combinations with all templates was within the range of 90–110% (Figure A2). We used the resulting mean efficiency value across all strains (95.8%) for all subsequent calculations of RiboJ autocatalytic activity. We assayed the efficiency of RiboJ autocatalytic activity using at least triplicates for each strain and promoter combination (Experimental procedures). RiboJ cutting efficiency was high in all cases. Overall we found that 98% of all mRNA molecules containing RiboJ were cleaved. This was extremely robust for almost all strain and promoter combinations, with the lowest median value being 97% (Figure 3). We also found that RiboJ activity was robust

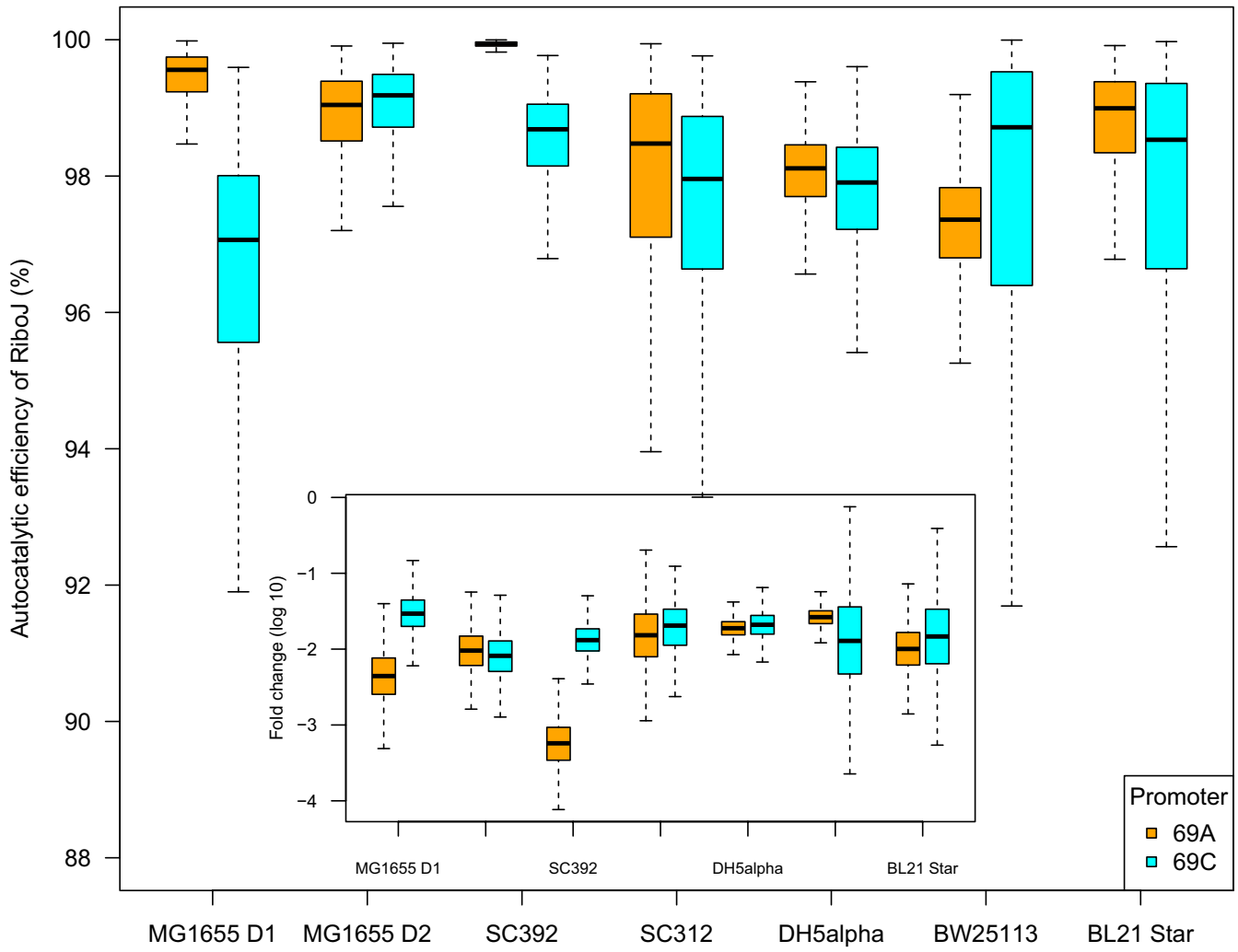

FIGURE 3 Autocatalytic efficiency of RiboJ. The boxplots in the figure show the minimum and maximum value (whiskers), the first and third quartile (boxes), and the median. These values were obtained through bootstrapping the RT-qPCR data (see Experimental procedures). D1 and D2 in MG1655 strain labels indicate that this data is from different biological replicates for which the RNA was extracted on different days (D1 and D2 denoting day 1 and day 2, respectively). The inset shows fold changes in the abundance of uncut transcripts with RiboJ relative to all transcripts. Note that the smaller range in cutting efficiency of RiboJ in SC392 strain for promoter 69A is simply a consequence of converting the C_t fold change of the two different amplicons into catalytic efficiency in percentages. The inset shows that the range and error in fold changes for SC392 with promoter 69A is comparable to the other samples

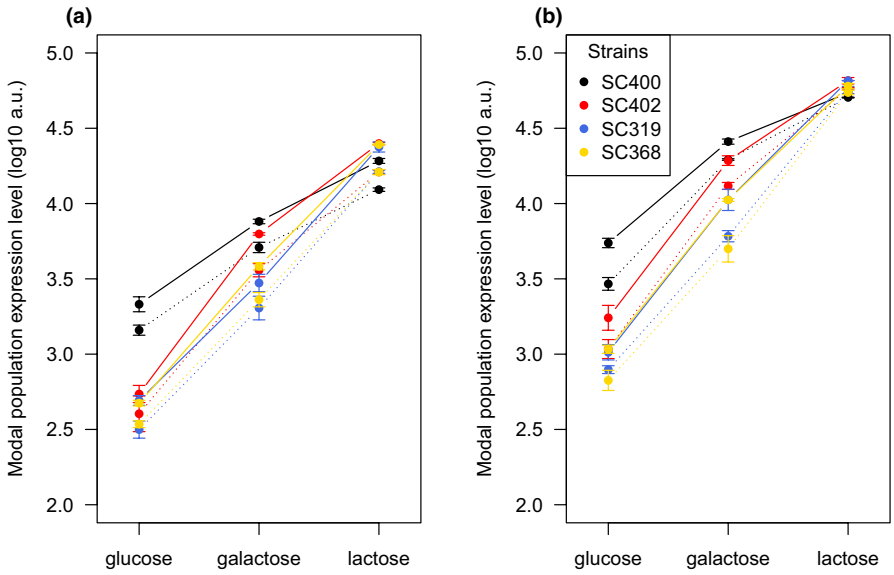

Figure A1 Modal expression levels differ consistently due to a single A to C change at position +69 of the *lacZ* open reading frame both without RiboJ (a) and with RiboJ (b) in additional strains. Shown are the modal population fluorescence levels for GFP driven by an upstream *lacZ* promoter for four additional *E. coli* strains in Figure 1. In all genetic backgrounds tested and all growth conditions (glucose, galactose, and lactose), the fluorescence levels from a promoter with the 69C polymorphism (dotted line) were consistently lower than those from the promoter with the 69A polymorphism (solid line). On the log10 scale that is shown, a 0.1 difference is equivalent to a 25% change in expression

to *cis*-changes, with no consistent differences between the 69A and 69C versions of the promoter.

However, we observed one exception to this robust behavior. In strain SC392, the 69A version of the promoter construct exhibited a 10-fold higher cutting efficiency (Figure 3, inset). To obtain an estimate of error for our measurements and test whether sampling alone could account for this or other differences, we bootstrapped the data 10,000 times and recalculated the efficiencies (Figure 3, Experimental procedures). We found that sampling alone was unlikely to account for the higher efficiency of 69A that we observed. We thus sequenced all plasmids from the SC392 strain to check for possible SNPs in the vector backbone that might lead to what we see as an increased RiboJ autocatalytic activity in this strain. We discovered single SNPs in each of the two plasmids with RiboJ. They were not identical, but each was located close to the origin of replication and thus could have affected the copy number of these plasmids. It is thus possible that the shift in RiboJ activity we observed for 69A in SC392 is due to a SNP in plasmid p69A.RJ+.

4 | DISCUSSION

Given the efficient activity of RiboJ (resulting in 98% of all mRNA molecules being cut), the differences in splicing measured between the two *lacZ* promoters and among the strains cannot explain the changes in expression we observed (Figure 1 and Figure A1). Rather than being due to the C69A SNP affecting the activity of RiboJ, the changes in expression are a consequence of this SNP affecting the regulation of both transcription and translation. The C69 SNP lowers both transcription and translation by approximately 25% (Figure 1 and Figure A1).

Considering the depth at which the activity of the *lacZ* promoter has been studied, we do not expect this SNP to be part of some unknown transcription factor binding site. The SNP may create a binding site causing a polymerase or transcription factor to pause during its linear search on the DNA strand for functional binding sites, thus inhibiting transcription. Processes such as transcriptional pausing and attenuation have been previously described in bacteria (Bailey et al., 2021; Blainey et al., 2006; Mustaev et al., 2017; Naville & Gautheret, 2009). These provide a more plausible explanation for the effect we see.

At the level of translational regulation, there is a possibility that the C69A SNP causes a difference in the secondary structure of the mRNA. This could then lead to differential accessibility of the mRNA to ribosomes. It is also possible that it inhibits proper translation by causing spurious ribosomal binding (Whitaker et al., 2015). However, it is beyond the scope of this paper to uncover the very mechanism of the regulation the SNP is involved in.

5 | CONCLUSION

In this study, we have confirmed that the autocatalytic activity of the ribozyme RiboJ is robust in *cis*- and *trans*-genetic contexts. This robust behavior of RiboJ suggests that the differences in expression that we observed in Figure 1 and Figure A1 are a result of changes in both transcription and translation due to the single C69A SNP, and not to changes in RiboJ autocatalytic efficiency. We note that

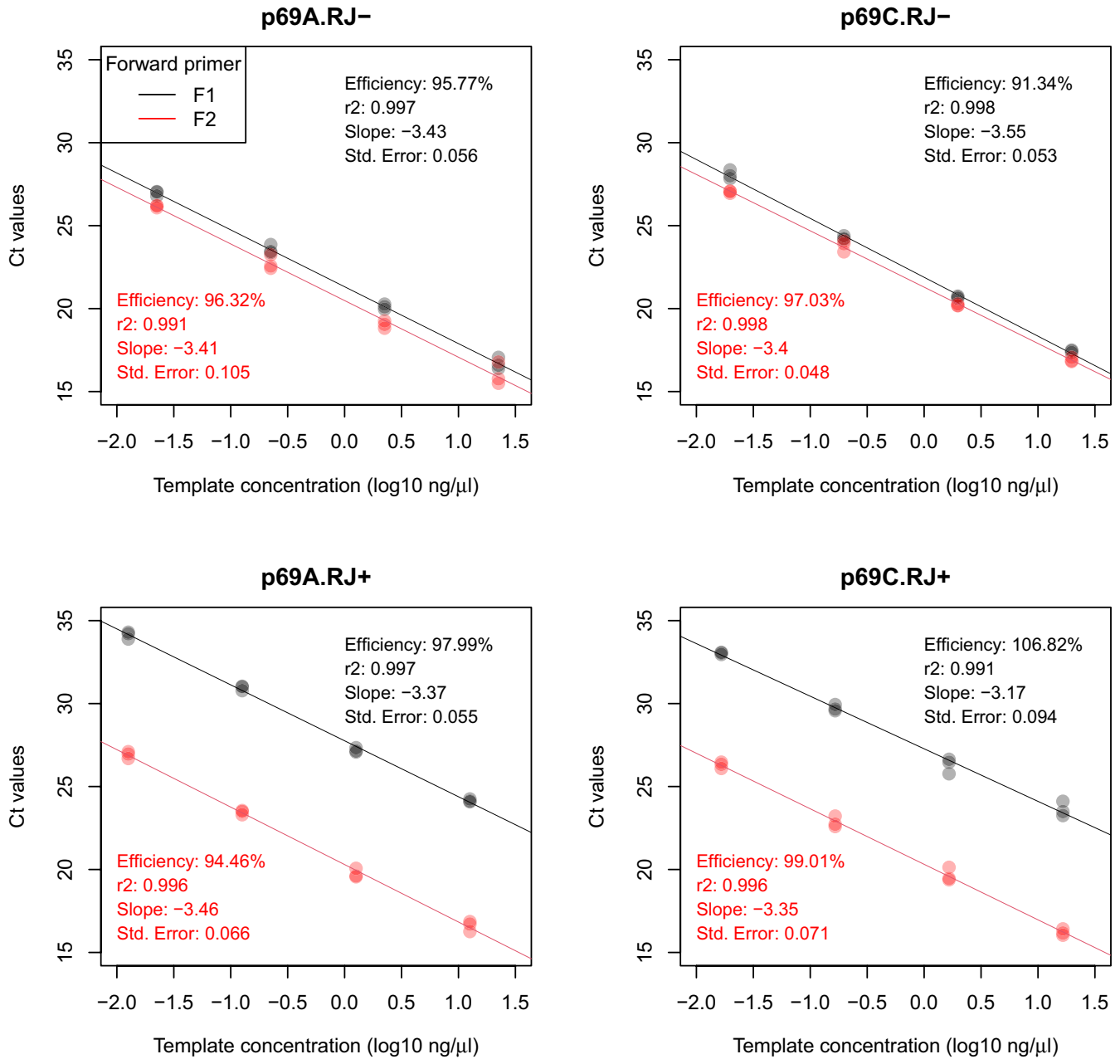

Figure A2 Amplification efficiency of all primer-template combinations. Each point indicates the C_t value for one technical replicate at different template concentrations, with each panel indicating one template and each color (red or black) indicating one primer combination. The lines show linear regressions, calculated using all data points for a given primer-template combination. For the templates without RiboJ (top panels), both primer pairs result in nearly equal C_t values. For the templates with RiboJ (bottom panels), the F1 primer pair has consistently larger C_t values, as expected. To calculate the catalytic activity of RiboJ, we used the mean amplification efficiency across all primer-template combinations, 95.8%.

there have been no previous reports that this region is involved in *lacZ* gene regulation. We proposed possible ways by which this SNP can be affecting both transcription and translation, however, more in-depth research is needed to determine the actual mechanism.

ACKNOWLEDGEMENTS

We would like to thank Tim Cooper for constructive input, D. Blank for providing p69A.RJ− and p69C.RJ− plasmids and Stella Pearless for plasmid preparation for Nanopore sequencing. This work was supported by the Royal Society Te Apārangi, Marsden Grant (MAU1703) awarded to Olin K. Silander. The funder had no role in study design, data collection, and interpretation, or the decision to submit the work for publication.

CONFLICT OF INTEREST

None declared.

AUTHOR CONTRIBUTIONS

Markéta Vlková: Conceptualization (equal); Data curation (lead); Formal analysis (lead); Investigation (equal); Methodology (lead); Project administration (supporting); Visualization (lead); Writing-original draft (lead); Writing-review & editing (equal). **Bhargava Reddy Morampalli:** Investigation (equal); Writing-review & editing (supporting). **Olin K. Silander:** Conceptualization (equal); Formal analysis (supporting); Funding acquisition (lead); Methodology (supporting); Project administration (lead); Resources (lead); Supervision (lead); Writing-original draft (supporting); Writing-review & editing (equal).

ETHICS STATEMENT

None required.

DATA AVAILABILITY STATEMENT

The original data files and scripts with data analysis that support the findings of this study are available in GitHub and accessible through the Zenodo repository at https://doi.org/10.5281/zenodo.5154246

ORCID

Markéta Vlková https://orcid.org/0000-0002-0272-5115
Bhargava Reddy Morampalli https://orcid.org/0000-0003-2741-6826
Olin K. Silander https://orcid.org/0000-0003-4105-8316

REFERENCES

Bailey, S. F., Alonso Morales, L. A., & Kassen, R. (2021). Effects of synonymous mutations beyond codon bias: The evidence for adaptive 4 synonymous substitutions from microbial evolution experiments. *Genome Biology and Evolution*, evab141. https://doi.org/10.1093/gbe/evab141

Barbier, I., Perez-Carrasco, R., & Schaerli, Y. (2020). Controlling spatiotemporal pattern formation in a concentration gradient with a synthetic toggle switch. *Molecular Systems Biology*, *16*(6), e9361. https://doi.org/10.15252/msb.20199361

Bartoli, V., Meaker, G. A., di Bernardo, M., & Gorochowski, T. E. (2020). Tunable genetic devices through simultaneous control of transcription and translation. *Nature Communications*, *11*(1), 2095. https://doi.org/10.1038/s41467-020-15653-7

Bittihn, P., Didovyk, A., Tsimring, L. S., & Hasty, J. (2020). Genetically engineered control of phenotypic structure in microbial colonies. *Nature Microbiology*, *5*(5), 697–705. https://doi.org/10.1038/s41564-020-0686-0

Blainey, P. C., van Oijen, A. M., Banerjee, A., Verdine, G. L., & Xie, X. S. (2006). A base-excision DNA-repair protein finds intrahelical lesion bases by fast sliding in contact with DNA. *Proceedings of the National Academy of Sciences of the United States of America*, *103*(15), 5752–5757. https://doi.org/10.1073/pnas.0509723103

Blattner, F. R., Plunkett, G., Bloch, C. A., Perna, N. T., Burland, V., Riley, M., Collado-Vides, J., Glasner, J. D., Rode, C. K., Mayhew, G. F., Gregor, J., Davis, N. W., Kirkpatrick, H. A., Goeden, M. A., Rose, D. J., Mau, B., & Shao, Y. (1997). The complete genome sequence of *Escherichia coli* K-12. *Science*, *277*(5331), 1453–1462. https://doi.org/10.1126/science.277.5331.1453

Breckell, G., & Silander, O. K. (2020). Complete genome sequences of 47 environmental isolates of *Escherichia coli*. *Microbiology Resource Announcements*, *9*(38), e00222-20. https://doi.org/10.1128/MRA.00222-20

Carrier, T. A., & Keasling, J. D. (1997). Engineering mRNA stability in *E. coli* by the addition of synthetic hairpins using a 5′ cassette system. *Biotechnology and Bioengineering*, *55*(3), 4. https://doi.org/10.1002/(SICI)1097-0290(19970805)55:3<577:AID-BIT16>3.0.CO;2-D

Clifton, K. P., Jones, E. M., Paudel, S., Marken, J. P., Monette, C. E., Halleran, A. D., Epp, L., & Saha, M. S. (2018). The genetic insulator RiboJ increases expression of insulated genes. *Journal of Biological Engineering*, *12*(1), 23. https://doi.org/10.1186/s13036-018-0115-6

Datsenko, K. A., & Wanner, B. L. (2000). One-step inactivation of chromosomal genes in *Escherichia coli* K-12 using PCR products. *Proceedings of the National Academy of Sciences*, *97*(12), 6640–6645. https://doi.org/10.1073/pnas.120163297

Gibson, D. G., Young, L., Chuang, R.-Y., Venter, J. C., Hutchison, C. A., & Smith, H. O. (2009). Enzymatic assembly of DNA molecules up to several hundred kilobases. *Nature Methods*, *6*(5), 343–345. https://doi.org/10.1038/nmeth.1318

Ishii, S., Ksoll, W. B., Hicks, R. E., & Sadowsky, M. J. (2006). Presence and growth of naturalized *Escherichia coli* in temperate soils from lake superior watersheds. *Applied and Environmental Microbiology*, *72*(1), 612–621. https://doi.org/10.1128/AEM.72.1.612-621.2006

Levskaya, A., Chevalier, A. A., Tabor, J. J., Simpson, Z. B., Lavery, L. A., Levy, M., Davidson, E. A., Scouras, A., Ellington, A. D., Marcotte, E. M., & Voigt, C. A. (2005). Engineering *Escherichia coli* to see light. *Nature*, *438*(7067), 441–442. https://doi.org/10.1038/nature04405

Li, C., Wen, A., Shen, B., Lu, J., Huang, Y., & Chang, Y. (2011). FastCloning: A highly simplified, purification-free, sequence- and ligation-independent PCR cloning method. *BMC Biotechnology*, *11*(1), 92. https://doi.org/10.1186/1472-6750-11-92

Lou, C., Stanton, B., Chen, Y.-J., Munsky, B., & Voigt, C. A. (2012). Ribozyme-based insulator parts buffer synthetic circuits from genetic context. *Nature Biotechnology*, *30*(11), 1137–1142. https://doi.org/10.1038/nbt.2401

Mustaev, A., Roberts, J., & Gottesman, M. (2017). Transcription elongation. *Transcription*, *8*(3), 150–161. https://doi.org/10.1080/21541264.2017.1289294

Na, D., Yoo, S. M., Chung, H., Park, H., Park, J. H., & Lee, S. Y. (2013). Metabolic engineering of Escherichia coli using synthetic small regulatory RNAs. *Nature Biotechnology*, *31*(2), 170–174. https://doi.org/10.1038/nbt.2461

Naville, M., & Gautheret, D. (2009). Transcription attenuation in bacteria: Theme and variations. *Briefings in Functional Genomics and Proteomics*, *8*(6), 482–492. https://doi.org/10.1093/bfgp/elp025

Neves, D., Vos, S., Blank, L. M., & Ebert, B. E. (2020). Pseudomonas mRNA 2.0: Boosting gene expression through enhanced mRNA stability and translational efficiency. *Frontiers in Bioengineering and Biotechnology*, *7*, 458. https://doi.org/10.3389/fbioe.2019.00458

Pfaffl, M. W. (2001). A new mathematical model for relative quantification in real-time RT-PCR. *Nucleic Acids Research*, *29*(9), 45e–445. https://doi.org/10.1093/nar/29.9.e45

Schmiedel, J. M., Carey, L. B., & Lehner, B. (2019). Empirical mean-noise fitness landscapes reveal the fitness impact of gene expression noise. *Nature Communications*, *10*(1), 3180. https://doi.org/10.1038/s41467-019-11116-w

Urtecho, G., Tripp, A. D., Insigne, K. D., Kim, H., & Kosuri, S. (2019). Systematic dissection of sequence elements controlling σ70 promoters using a genomically encoded multiplexed reporter assay in *Escherichia coli*. *Biochemistry*, *58*(11), 1539–1551. https://doi.org/10.1021/acs.biochem.7b01069

Whitaker, W. R., Lee, H., Arkin, A. P., & Dueber, J. E. (2015). Avoidance of truncated proteins from unintended ribosome binding sites within heterologous protein coding sequences. *ACS Synthetic Biology*, *4*(3), 249–257. https://doi.org/10.1021/sb500003x

Yu, H., Wang, Z., Xu, H., Guo, J., Ma, Q., Mu, X., & Luo, Y. (2018). A method for absolute protein expression quantity measurement employing insulator RiboJ. *Engineering*, *4*(6), 881–887. https://doi.org/10.1016/j.eng.2018.09.012

Zaslaver, A., Bren, A., Ronen, M., Itzkovitz, S., Kikoin, I., Shavit, S., Liebermeister, W., Surette, M. G., & Alon, U. (2006). A comprehensive library of fluorescent transcriptional reporters for *Escherichia coli*. *Nature Methods*, *3*(8), 623–628. https://doi.org/10.1038/nmeth895

How to cite this article: Vlková, M., Morampalli, B. R., & Silander, O. K. (2021). Efficiency of the synthetic self-splicing RiboJ ribozyme is robust to *cis*- and *trans*-changes in genetic background. *MicrobiologyOpen*, 10, e1232. https://doi.org/10.1002/mbo3.1232

APPENDIX A

TABLE A1 Primers and oligos used in this work

Primer or oligo ID	Sequence	Purpose
pUA66_insert_F3965	5′ - TTG TCT GTT GTG CCC AGT CAT AGC -3′	PCR & Sanger sequencing
pUA66_insert_R232	5′- TCG CAA AGC ATT GAA GAC CAT ACG C -3′	PCR & Sanger sequencing
RiboJ_oligo1_Rev	5′ - GAA AGC ACA TCC GGT GAC AGC TGG ATC CCC TCG AGG TGA AGA CGA AAG GGC CTC GTG ATA - 3′	DNA assembly of pMV001
RiboJ_oligo2_For	5′ - GGG GAT CCA GCT GTC ACC GGA TGT GCT TTC CGG TCT GAT GAG TCC GTG AGG ACG AAA CAG - 3′	DNA assembly of pMV001
RiboJ_oligo3_Rev	5′ - TCT TAG TTT AAA CAA AAT TAT TTG TAG AGG CTG TTT CGT CCT CAC GGA CTC ATC AGA CCG - 3′	DNA assembly of pMV001
RiboJ_oligo4_For	5′ - CCT CTA CAA ATA ATT TTG TTT AAA CTA AGA AGG AGA TAT ACA TAT GAG TAA AGG AGA - 3′	DNA assembly of pMV001
pUA66_vector_F	5′ - GAA GGA GAT ATA CAT ATG AGT AAA GG - 3′	PCR of pUA66 for DNA assembly of pMV001 & RT-qPCR assay (**primer F2**)
pUA66_vector_R	5′ - TCG AGG TGA AGA CGA AAG G - 3′	PCR of pUA66 for DNA assembly of pMV001
pMV001_FastClonV_F	5′ - AGC TGT CAC CGG ATG TGC - 3′	PCR of pMV001 for DNA assembly of p69A.RJ+ and p69C.RJ+
pMV01_FastClonV_R	5′ - TCG AGG TGA AGA CGA AAG GGC - 3′	PCR of pMV001 for DNA assembly of p69A.RJ+ and p69C.RJ+
lacZ_FastClonIN_F	5′ - **TTT CGT CTT CAC CTC GA**C AAT ACG CAA ACC GCC TCT CC - 3′	PCR of p69A.RJ− and p69C.RJ− for DNA assembly of p69A.RJ+ and p69C.RJ+
lacZ_FastClonIN-D9_R	5′ - **CAC ATC CGG TGA CAG CT**G TGT AAC GCC AGG GTT TTC C - 3′	PCR of p69A.RJ− for DNA assembly of p69A.RJ+
lacZ_FastClonIN-K12_R	5′ - **CAC ATC CGG TGA CAG CT**G GGT AAC GCC AGG GTT TTC C - 3′	PCR of p69C.RJ− for DNA assembly of p69C.RJ+
lacZ_qPCR_F	5′ - ATG ATT ACG GAT TCA CTG GC - 3′	RT-qPCR assay (**primer F1**)
GFP_qPCR_R	5′ - GAA AAT TTG TGC CCA TTA ACA TCA CC - 3′	RT-qPCR assay (**primer R**)
GFP_Probe	5′ - /56-FAM/TTC AAC AAG/ZEN/AAT TGG GAC AAC TCC AGT GAA AAG TT/3IABkFQ/ - 3′	RT-qPCR assay (**probe**)

Note: Bold sequences = regions homologous to PCR amplified pMV001 vector. Primers and the probe used for RT-qPCR assay are highlighted in bold with their simplified names that were used in the main text and Figure 2 (Purpose column).